NMR Structure and Molecular Dynamics of the In-Plane Membrane Anchor of Nonstructural Protein 5A from Bovine Viral Diarrhea Virus † , ‡

ARTICLE *in* BIOCHEMISTRY · MARCH 2006

Impact Factor: 3.02 · DOI: 10.1021/bi0517685 · Source: PubMed

NMR Structure and Molecular Dynamics of the In-Plane Membrane Anchor of Nonstructural Protein 5A from Bovine Viral Diarrhea Virus[†,‡]

Nicolas Sapay,[§] Roland Montserret,[§] Christophe Chipot,[||] Volker Brass,[⊥] Darius Moradpour,[#] Gilbert Deléage,[§] and François Penin*[,§]

Institut de Biologie et Chimie des Protéines, CNRS-UMR 5086, IFR128 BioSciences Lyon-Gerland, University of Lyon, F-69367 Lyon, France, Institut Nancéien de Chimie Moléculaire, CNRS-UMR 7565, University of Nancy I, BP 239, F-54506 Vandoeuvre-lès-Nancy Cedex, France, Department of Medicine II, University of Freiburg, Hugstetter Strasse 55, D-79106 Freiburg, Germany, and Division of Gastroenterology and Hepatology, Centre Hospitalier Universitaire Vaudois, University of Lausanne, Rue du Bugon 46, CH-1011 Lausanne, Switzerland

Received September 1, 2005; Revised Manuscript Received December 19, 2005

ABSTRACT: Hepatitis C virus (HCV) nonstructural protein 5A (NS5A) is a monotopic membrane protein anchored to the membrane by an N-terminal in-plane amphipathic α-helix. This membrane anchor is essential for the assembly of a functional viral replication complex. Although amino acid sequences differ considerably, putative membrane anchors with amphipathic features were predicted in NS5A from related Flaviviridae family members, in particular bovine viral diarrhea virus (BVDV), the prototype representative of the genus *Pestivirus*. We report here the NMR structure of the membrane anchor 1−28 of NS5A from BVDV in the presence of different membrane mimetic media. This anchor includes a long amphipathic α-helix of 21 residues interacting in-plane with the membrane interface and including a putative flexible region. Molecular dynamic simulation at a water−dodecane interface used to mimic the surface separating a lipid bilayer and an aqueous medium demonstrated the stability of the helix orientation and the location at the hydrophobic−hydrophilic interface. The flexible region of the helix appears to be required to allow the most favorable interaction of hydrophobic and hydrophilic side chain residues with their respective environment at the membrane interface. Despite the lack of amino acid sequence similarity, this amphipathic helix shares common structural features with that of the HCV counterpart, including a stable, hydrophobic N-terminal segment separated from the more hydrophilic C-terminal segment by a local, flexible region. These structural conservations point toward conserved roles of the N-terminal in-plane membrane anchors of NS5A in replication complex formation of HCV, BVDV, and other related viruses.

Nonstructural protein 5A (NS5A)[1] from bovine viral diarrhea virus (BVDV) and that from hepatitis C virus (HCV) are phosphorylated proteins of unknown function (*1*, *2*). In HCV, it is found in a 56 kDa basally phosphorylated form and in a 58 kDa hyperphosphorylated form. The phosphorylation state of NS5A was recently proposed to have a regulatory function in HCV RNA replication (*3*−*5*). NS5A is believed to be an essential component of the HCV replication complex. Numerous additional functions and a plethora of interaction partners have been postulated for NS5A (reviewed in refs *6* and *7*), including the modulation of cellular interferon responses (reviewed in ref *8*). However, the definitive function of NS5A is elusive, and surprisingly little effort has been devoted to the basic biochemical characterization of this protein.

A characteristic feature of positive-strand RNA viruses such as HCV is that the nonstructural proteins form a membrane-associated replication complex together with replicating viral RNA, altered membranes, and additional as yet largely unidentified host cell components (*9*, *10*). In this context, we (*11*) and others (*12*) demonstrated that the N-terminal segment of residues 1−31 of NS5A from HCV mediates posttranslational membrane association of NS5A.

[†] This work was supported by the French Centre National de la Recherche Scientifique (CNRS, F.P. and G.D.), by European Commission Grants QLK2-CT2002-01329 and LSHM-CT-2004-503359 (VIRGIL European Network of Excellence on Antiviral Drug Resistance) (to F.P., G.D., and D.M.), by the Agence Nationale de Recherches sur le SIDA et les Hépatites Virales (ANRS) (F.P.), by Grant 3100A0-107831/1 from the Swiss National Science Foundation (to D.M.), and by Grant 04C59 from the Novartis Foundation (to D.M.). N.S. is the recipient of a BDI doctoral fellowship from the French CNRS.

[‡] The atomic coordinates and structure factors (entries 2AJJ, 2AJM, 2AJN, and 2AJO) have been deposited in the Protein Data Bank. The corresponding proton and carbon chemical shifts have been deposited in the BioMagResBank as accession number 6757.

* To whom correspondence should be addressed: IBCP-CNRS UMR5086, 7, Passage du Vercors, F-69367 Lyon, Cedex 07, France. Phone: 33 472 722 648. Fax: 33 472 722 604. E-mail: f.penin@ibcp.fr.

[§] University of Lyon.

[||] University of Nancy I.

[⊥] University of Freiburg.

[#] University of Lausanne.

[1] Abbreviations: 3D, three-dimensional; aa, amino acid(s); BVDV, bovine viral diarrhea virus; DPC, dodecylphosphocholine; ER, endoplasmic reticulum; GFP, green fluorescent protein; HCV, hepatitis C virus; HSQC, heteronuclear single-quantum coherence spectroscopy; MD, molecular dynamics; NOESY, nuclear Overhauser effect spectroscopy; NMR, nuclear magnetic resonance; NS5A, nonstructural protein 5A; NS5A[1−28], aa 1−28 of NS5A; rmsd, root-mean-square deviation; POPC, 1-palmitoyl-2-oleoyl-3-*sn*-glycero-3-phosphocholine; RP-HPLC, reverse-phase high-performance liquid chromatography; SDS, sodium dodecyl sulfate; TFE, 2,2,2-trifluoroethanol; TOCSY, total correlation spectroscopy.

10.1021/bi0517685 CCC: $33.50
Published on Web 01/31/2006

Our recent NMR structure analyses demonstrated that membrane anchorage is due to the embedding of a long amphipathic α-helix at the membrane interface (*13*). This helix (amino acids 5−25) displays a hydrophobic, tryptophan-rich side interacting with the hydrophobic core of the phospholipid bilayer, while the polar, charged side is exposed to the cytosol. Thus, NS5A is a monotopic membrane protein exhibiting an in-plane amphipathic α-helix as a membrane anchor located at its amino terminus (*11*, *13*). Functional analyses demonstrated that this helix defines a platform probably involved in specific protein−protein interactions essential for the formation of a functional HCV replication complex (*13*). Limited proteolysis of recombinant NS5A has allowed the organization of this protein in three domains downstream of the membrane-anchoring amphipathic α-helix to be specified (*2*). Recently, Tellinghuisen et al. (*14*) reported the X-ray structure at 2.5 Å resolution of the relatively highly conserved domain I which forms dimers associated by the N-terminal ends of the molecules. Since only five residues are missing between the membrane-anchoring amphipathic α-helix and domain I, it is probable that the N-terminus of domain I is located close to the membrane. The basic nature of the surface of N-terminal domain I led the authors to propose that it could interact with the negatively charged phospholipid headgroups on the membrane surface. This interaction would position a groove generated by the "claw-like" dimer facing away from the membrane, where it could interact with RNA (*14*).

We recently studied the determinants for membrane association of NS5A from HCV-related Flaviviridae family members (V. Brass, Z. Pal, N. Sapay, H. E. Blum, F. Penin, and D. Moradpour, submitted for publication). This family comprises the genera *Flavivirus*, *Hepacivirus*, and *Pestivirus* as well as the yet unassigned GB viruses A (GBV-A), GBV-B, and GBV-C. A wide range of diseases is induced by these viruses in humans (e.g., hemorrhagic fever or encephalitis for genus *Flavivirus* and hepatitis C for genus *Hepacivirus*) or in animals [e.g., fatal mucosal disease for BVDV, the prototype representative of the genus *Pestivirus* (*15*)]. All of these viruses are enveloped positive-strand RNA viruses exhibiting a similar overall genome organization (see Figure 1A) and expressing their structural and nonstructural proteins via translation of a single open reading frame (*16*). Although primary amino acid (aa) sequences differed considerably, putative membrane anchors with amphipathic features were predicted in the N-terminal sequences of NS5A from BVDV, GBV-B, and GBV-C (V. Brass et al., submitted for publication). By confocal laser scanning microscopy as well as membrane sedimentation and flotation analyses, these proteins exhibited membrane association characteristics very similar to those of HCV NS5A. Analyses of GFP fusion constructs revealed that the N-terminal segments of residues 1−27 to 1−33 of these NS5A proteins were sufficient for membrane association (segment 1−28 for BVDV; see Figure 1). Circular dichroism analyses of synthetic peptides representing these membrane anchors confirmed their α-helical structure. We concluded that membrane association of NS5A with an N-terminal amphipathic α-helix is a feature shared by HCV and related members of the Flaviviridae family. This observation further supports the relevance of these viruses as model systems for HCV and points toward conserved roles of the N-terminal amphipathic α-helices of NS5A in replication complex formation. This conservation may be exploited in the search for cellular factors involved in HCV RNA replication and in the development and evaluation of novel antiviral strategies.

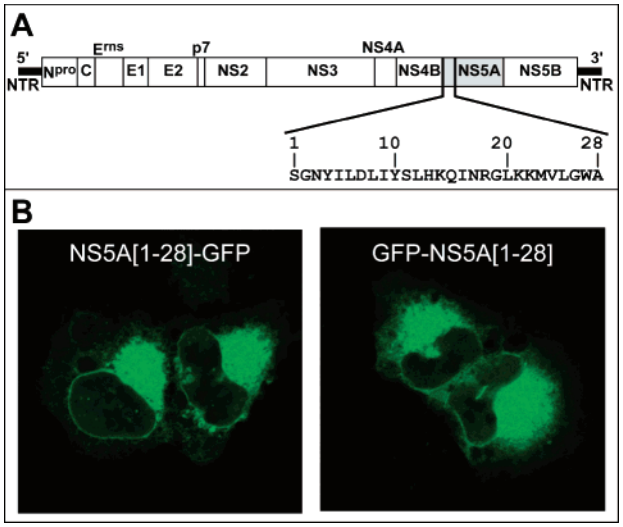

FIGURE 1: Genome organization of bovine viral diarrhea virus (BVDV) and association of its NS5A N-terminal sequence of residues 1−28 with the ER membrane. (A) The BVDV genome is a single-stranded RNA with positive polarity of 12.6 kb (*57*), and its organization is similar to that of HCV (*58*). The single encoded polyprotein precursor is co- and post-translationally processed by cellular and viral proteases to yield the mature structural and nonstructural proteins. For both BVDV and HCV, the structural proteins include the core protein (C) and envelope glycoproteins E1 and E2, and an additional envelope protein E0 with associated RNase activity (E^{rns}) for BVDV (*59*). In addition, the N-terminus of the BVDV polyprotein includes the protein N^{pro} that ensures the release of the core protein by autoproteolysis (*60*). For both viruses, the nonstructural proteins include NS2-3 autoprotease, NS3 protein composed of an N-terminal serine protease domain and a C-terminal RNA helicase domain, NS4A membrane polypeptide NS3 cofactor, NS4B membrane protein, NS5A, and NS5B RNA-dependent RNA polymerase. NS5A is colored gray, and its N-terminal membrane anchor of aa 1−28 studied here is indicated (GenBank accession number M31182). (B) Confocal laser scanning microscopy views showing the subcellular distribution of the green fluorescent protein (GFP) fused to N-terminal aa 1−28 of BVDV NS5A expressed in U2-OS cells (V. Brass et al., submitted for publication). The BVDV NS5A[1−28] sequence fused to either the N- or C-terminus of GFP (NS5A[1−28]−GFP and GFP−NS5A-[1−28] panels) is sufficient to target this protein to endoplasmic reticulum membranes, while GFP expressed alone is diffusely distributed in the cytoplasm and nucleus (see Figure 2 of ref *11*).

Monotopic membrane proteins constitute a particular class of protein which binds to the surface of the membrane. However, detailed three-dimensional structures are known for only four protein types listed as monotopic in the Membrane Protein Resource (http://blanco.biomol.uci.edu/Membrane_Proteins_xtal.html). The parts of the proteins located in the membrane interface region have received limited attention, and the structural constraints imposed on the proteins by this region of the phospholipid bilayer remain poorly documented (*17*). Thus, the positioning of in-plane amphipathic helices at the membrane interface remains poorly understood, and molecular dynamics (MD) in membrane mimetic environments is an attractive tool for gaining further insight (*18*, *19*).

In this study, we have investigated the structure of the NS5A membrane anchor from BVDV which presents no

obvious aa conservation with its HCV counterpart. The three-dimensional structure of a synthetic peptide corresponding to this membrane anchor, NS5A[1−28], was determined by NMR in the presence of sodium dodecyl sulfate (SDS) or trifluoroethanol (TFE, 50%) used to mimic the membrane environment. NMR data revealed the presence of a long amphipathic α-helix and support an in-plane interaction with the membrane bilayer interface. In addition, this helix shares common structural features with that of the HCV counterpart. The positioning of this amphipathic helix at the membrane interface and its flexibility suggested by the NMR data were investigated by using molecular dynamics simulations at a water−dodecane interface. We report that the helix backbone is very likely located at the polar headgroup−alkyl chain interface of phospholipids and that the local flexibility of the helix appears to be required to allow the most favorable interaction of hydrophobic and hydrophilic side chain residues with their respective environment. These studies allowed us to propose a model of the positioning of the NS5A membrane anchor from BVDV.

EXPERIMENTAL PROCEDURES

Sequence Analysis. BVDV NS5A full-length sequences where retrieved from the UniProt protein database (*20*) using the BLAST homology search program (*21*). HCV NS5A sequences were retrieved from the European HCV database developed by our laboratory (http://euhcvdb.ibcp.fr/) (*22*) using BLAST. Multiple-sequence alignments were performed with CLUSTAL W (*23*) using default parameters. The repertoire of residues at each aa sequence position and their frequencies observed in natural sequence variants were computed by using a program developed by our laboratory (F. Dorkeld, C. Combet, F. Penin, and G. Deleage, unpublished data).

Confocal Laser Scanning Microscopy. Confocal laser scanning microscopy was performed as described previously (*11*). In brief, U-2 OS human osteosarcoma cells were grown on coverslips and transiently transfected with the pCMV-BVDV-5AN28-GFP or pCMV-GFP-BVDV-5AN28 plasmid that allows expression of the 28 N-terminal amino acids of BVDV NS5A fused to either the N- or C-terminus of the green fluorescent protein (V. Brass et al., submitted for publication). Cells were fixed with 2% paraformaldehyde and mounted in SlowFade (Molecular Probes, Eugene, OR). Slides were analyzed with a Zeiss LSM 510 confocal microscope, and images were processed with Adobe Photoshop version 7.0.

Peptide Synthesis. The NS5A[1−28] peptide, representing the first 28 N-terminal residues of NS5A from the BVDV 1 isolate NADL (GenBank accession number M31182), was synthesized by the stepwise solid-phase method of Merrifield and by employing Fmoc chemistry. After cleavage and deprotection, the peptide was purified by RP-HPLC and exhibited the expected mass of 3200 Da when measured by electrospray mass spectrometry.

NMR Spectroscopy. For the NMR sample in 50% TFE-d_2 (>99% isotopic enrichment), the lyophilized NS5A[1−28] purified peptide was dissolved at a concentration of 2 mM (pH 4.5). For NMR samples in SDS-d_{25} (>98% isotopic enrichment) or dodecylphosphocholine (DPC)-d_{38} (>98% isotopic enrichment), the lyophilized peptide was dissolved in a 95/5 mixture of H_2O and D_2O containing 100 mM detergent to a final peptide concentration of 2 mM (pH 4.5 and 4.8 in SDS and DPC, respectively). DSS (2,2-dimethyl-2-silapentane-5-sulfonic acid) was used as an internal ^{1}H and ^{13}C chemical shift reference in all NMR samples.

NMR experiments in 50% TFE-d_2 were recorded in nonspinning mode at 303 and 313 K. Multidimensional NMR experiments were carried out at 500 MHz on a Varian Unity-*plus* spectrometer equipped with a triple-resonance proton−carbon−nitrogen 5 mm probe with a self-shielded *z* gradient coil and *ultra-nmr* shims. Nuclear Overhauser effect spectroscopy (NOESY), double-quantum-filtered correlation spectroscopy, homonuclear total correlation spectroscopy (TOCSY), and ^{1}H−^{13}C heteronuclear single-quantum correlation (HSQC) experiments using conventional optimized pulse sequences were performed as described previously (*24*−*26* and references therein). NOESY spectra were recorded with mixing times ranging from 50 to 150 ms, and an isotropic mixing time of 80 ms was used for clean-TOCSY (spectral window of 11 ppm, 2048 data points in F_2, and 256 or 512 increments in F_1). Varian VNMR software was used to process all data, and Sparky (from T. D. Goddard and D. G. Kneller, University of California, San Francisco, available at www.cgl.ucsf.edu/home/sparky) was used for analysis of two-dimensional spectra. Intraresidue backbone resonances and aliphatic side chains were identified from two-dimensional (2D) ^{1}H TOCSY and confirmed with ^{1}H−^{13}C HSQC in ^{13}C natural abundance. Sequential assignments were determined by correlating intraresidue assignments with interresidue cross-peaks observed in 2D ^{1}H NOESY. NMR-derived ^{1}Hα and ^{13}Cα chemical shifts are reported relative to the random coil chemical shifts in TFE (*27*, *28*).

For H−D exchange experiments, the peptide lyophilized in the presence of SDS was solubilized in 100% D_2O and fast NOESY spectra were recorded at appropriate time intervals over the course of 72 h. To confirm observed H−D exchange, this SDS/peptide sample was lyophilized again prior to solubilization in 100% H_2O, and again fast NOESY spectra were recorded over a period of 72 h. Fast NOESY spectra were recorded with a mixing time of 100 ms.

NMR-Derived Constraints and Structure Calculations. NOE intensities used as input for the structure calculations were obtained from the NOESY spectrum recorded with a 100 ms mixing time and checked for spin diffusion with spectra recorded with shorter mixing times (50 ms). NOEs were partitioned into three categories of intensities that corresponded to distances ranging from a common lower limit of 1.8 Å to upper limits of 2.8, 3.5, and 4.5 Å for strong, medium, and weak intensities, respectively. The cross-peak intensities of the Hδ−Hϵ protons of Tyr10 were used as the reference distance (2.45 Å). Neither dihedral angle nor hydrogen bond restraints were introduced. Protons without stereospecific assignments were treated as pseudoatoms, and the correction factors were added to the upper and lower distance constraints (*29*). Three-dimensional structures were generated from NOE distance constraints by the restrained dynamical simulated annealing protocol with XPLOR−NIH version 2.0.6 (*30*) using standard force fields and default parameter sets. Sets of 50 structures were calculated to widely sample the conformational space, and structures with no distance restraint violations (>0.5 Å) were retained. The selected structures were compared by pairwise root-mean-square deviation (rmsd) over the backbone atom coordinates

(N, Cα, and C′). Local analogies were analyzed by calculating the local rmsd of a tripeptide window sliding along the sequence. Statistical and structural analyses were performed using AQUA version 3.2 and PROCHECK-NMR version 3.5.4 (*31*).

Molecular Dynamics Simulations. Molecular dynamics (MD) simulations were performed in the isobaric−isothermal ensemble using NAMD version 2.5 (*32*). The trajectories were analyzed with the NAMD LogParser 1.0 (available at http://namd-lp.sourceforge.net/) and Ptraj (available at www.chpc.utah.edu/∼cheatham/software.html) utility codes. The MDTools 0.62 python module (available at www.ks.uiuc.edu/∼jim/mdtools/) has been used additionally to compute atom densities and first-order hydrophobic moments (*33*). The hydrophobic moment was computed using the Eisenberg hydrophobicity scale (*34*). Eight-state secondary structure assignment has been computed using Stride (*35*). Image rendering was carried out with VMD version 1.8.2 (*36*).

System Setup. The simulation cell consisted of one pre-equilibrated dodecane lamella in equilibrium between two lamellae of water as detailed previously (*37*). The NS5A-[1−28] average structure obtained in 50% TFE (PDB entry 2AJN) was placed slightly above the water−dodecane interface. The initial dimensions of the cell were 50 Å × 50 Å × 75 Å. The complete system included 2926 water molecules, 892 dodecane molecules, and the NS5A[1−28] peptide, representing a total of 4288 atoms. The peptide N-terminus was treated as a charged ammonium moiety and its C-terminus as a carboxyl group. The histidine was protonated at the Nδ1 site. The net charge of the peptide equal to +3 was neutralized by three chlorine counterions. The setup of the system and energy minimization were completed with CHARMM 27 (*38*).

Simulation Parameters. All simulations were carried out by employing the CHARMM27 force field (*39*). The system was simulated using periodic boundary conditions with a short-range cutoff radius of 12 Å. Long-range electrostatic interactions were handled with the particle mesh Ewald (PME) method (*40*, *41*). All bonds between hydrogen and heavy atoms were fixed to their equilibrium value. The equations of motion were integrated with a multiple-time step algorithm and a time step of 2 fs. The temperature and the pressure were fixed at 300 K and 1 bar, respectively, using Langevin dynamics and the Langevin piston method. The system was equilibrated over a period of 2 ns, followed by production for 6 ns.

RESULTS

NMR Structure of the BVDV NS5A[1−28] Peptide in Membrane Mimetic Media. Circular dichroism analyses of the BVDV NS5A[1−28] synthetic peptide performed in the presence of various membrane mimetic media such as SDS or DPC detergent micelles or TFE/water mixtures showed an α-helix content of ∼84% (V. Brass et al., submitted for publication). Here, the conformational behavior of NS5A-[1−28] in these commonly used membrane mimetic solvents for structure analysis of membrane peptides (*42*) was further investigated by NMR to gain insights into peptide folding at the atomic level. As illustrated by the NOESY spectral extracts of the Cα-NH region shown in Figure 2, the 2D

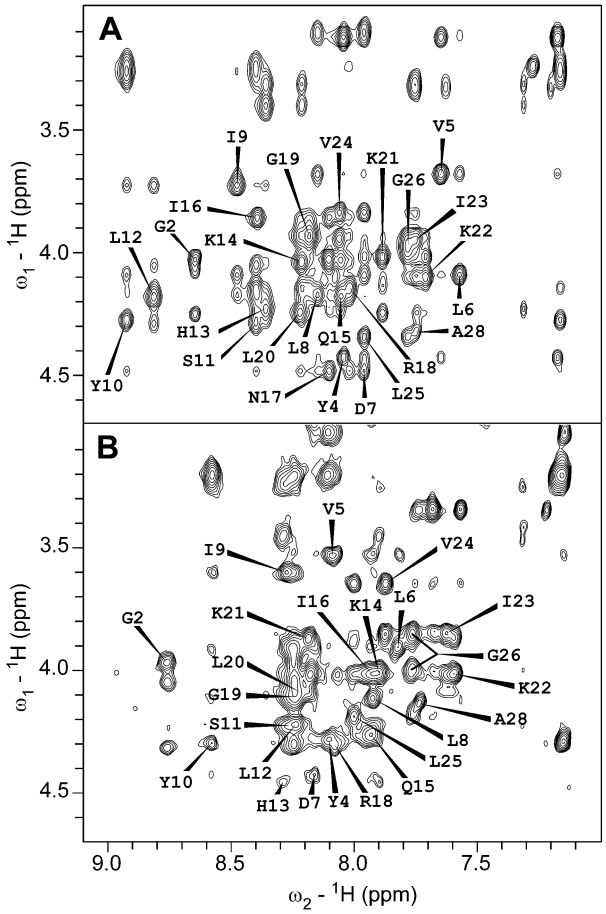

FIGURE 2: Extracts of the NOESY spectra of BVDV NS5A[1−28]. NH−Hα region of 2 mM NS5A[1−28] in 50% TFE (A) and 100 mM SDS (B) recorded at 303 K with a mixing time of 150 ms. NH−Hα intraresidue cross-peaks are labeled by residue number. Note that in 100 mM SDS (B), each of the two Hα resonances of Gly26 is observed.

homo- and heteronuclear NMR experiments with BVDV NS5A[1−28] dissolved in 50% TFE-d_2 or 100 mM SDS-d_{25} yielded well-resolved spectra (panels A and B of Figure 2, respectively). The spin systems were identified with TOCSY spectra at 298 and 308 K with the help of ^{1}H−^{13}C HSQC spectra in natural abundance. The sequential assignment was performed with the help of the NOESY spectrum obtained with a mixing time of 150 ms and temperatures of 298 and 308 K. Despite the poor dispersion of the NH and Hα resonances (25 of 28 HN and Hα resonances are spread over a range from 0.9 to 0.6 ppm, respectively), the sequential assignment of all spin systems was completed in 50% TFE (Figure 3A, left). The ^{1}H−^{13}C HSQC experiment allowed the confirmation of all proton side chain resonances as well as the determination of the ^{13}C resonances and calculation of the chemical shift differences for ^{1}Hα and ^{13}Cα (Figure 3B,C). The intensities of NOE cross-peaks were defined from the NOESY spectrum recorded at 298 K with a mixing time of 100 ms. Few side chain NOE cross-peaks were defined from the NOESY spectrum recorded at 208 K. NOESY spectra of the peptide in SDS-d_{25} micelles exhibited broader resonances and narrower dispersion of the NH and Hα resonances, as illustrated in Figure 2B. These spectra were however sufficiently well-resolved to allow the assignment of all spin systems, whereas the sequential assignment was only partially performed due to overlapping

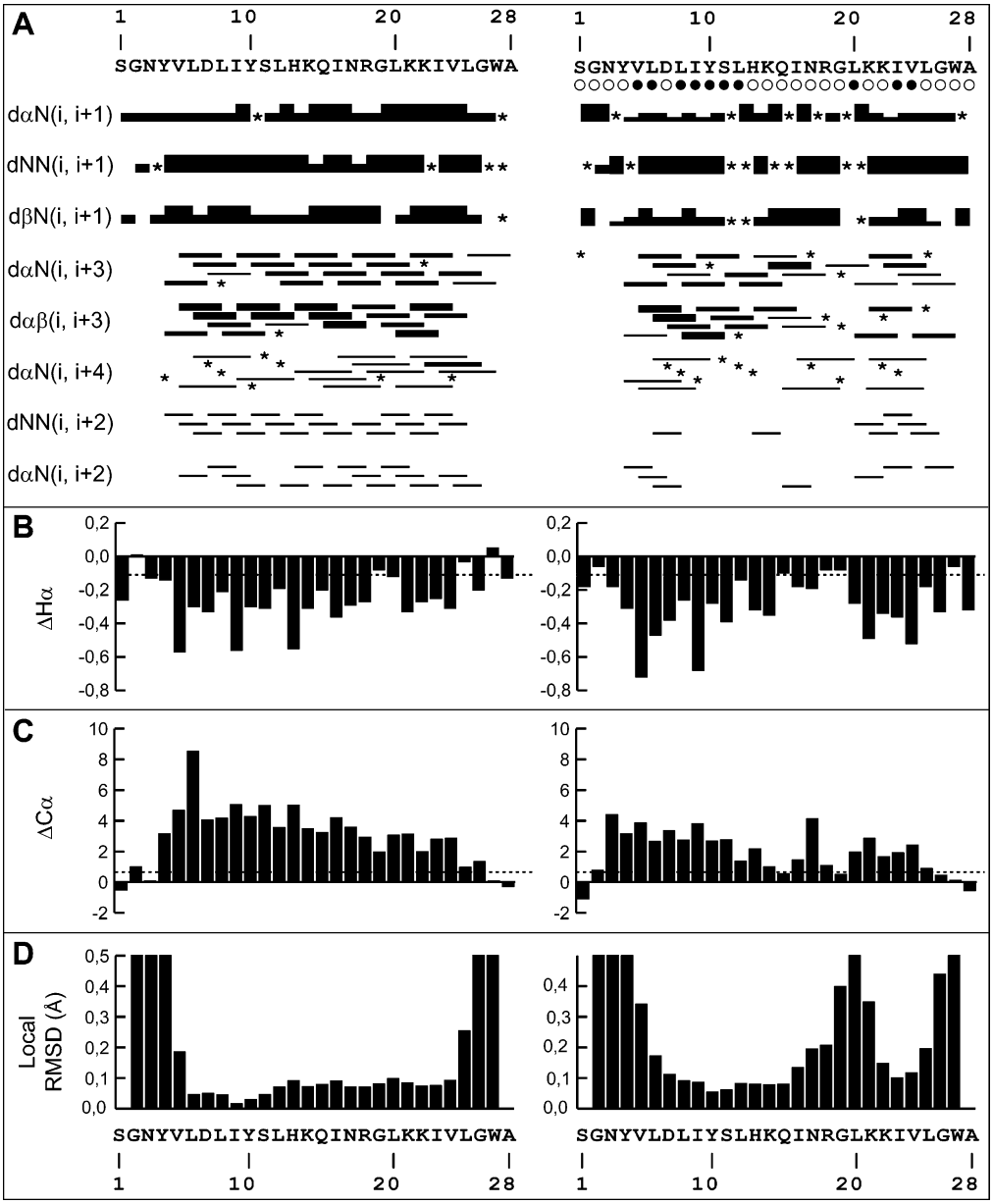

FIGURE 3: NMR analysis of BVDV NS5A[1−28]. (A) Summary of sequential (i, $i + 1$) and medium-range (i, $i + 2$ to i, $i + 4$) NOEs in 50% TFE (left) and 100 mM SDS (right). Intensities of NOEs are indicated by the height of the bars. Asterisks indicate that the presence of a NOE cross-peak that is not confirmed because of overlapping resonances. Amide protons that remained observable in a NOESY spectrum in 100 mM SDS after 14 h in D_2O are denoted with filled circles (very slowly exchangeable protons), while those disappearing within 14 h are denoted with empty circles (highly exchangeable protons). (B and C) ^{1}Hα and ^{13}Cα chemical shift differences (in parts per million) in 50% TFE (left) and 100 mM SDS (right), respectively. Chemical shift difference were calculated by subtraction of the experimental values from the random coil conformation values reported in refs *27* and *28* and corrected using sequence-dependent correction (*27, 28*). The dashed lines indicate the standard threshold value for an α-helix for ΔHα (−0.1 ppm) and ΔCα (0.7 ppm). (D) Histogram of the averaged rmsd values (i.e., local rmsd) of three residues for the backbone atoms of the final set of calculated structures in 50% TFE (left) and 100 mM SDS (right). Note that the corresponding structures are reported in Figure 4.

cross-peaks (Figure 3A, right). In contrast, for the peptide in dodecylphosphocholine (DPC-d_{38}) micelles, the broadening and overlapping of NMR cross-peaks were too large to complete the assignments (data not shown).

The overview of the sequential and medium-range NOE connectivities in 50% TFE (Figure 3A, left) shows that the main body of the peptide (residues 5−25) displays typical α-helix NOEs, including strong $d_{NN}(i, i + 1)$ sequential connectivities and weak $d_{NN}(i, i + 2)$, medium and strong $d_{\alpha\beta}(i, i + 3)$, and weak $d_{\alpha N}(i, i + 4)$ medium-range connectivities. In contrast, residues flanking the N- and C-terminal ends of the 5−25 helix remain more flexible with fewer or even no medium-range connectivities. This is the sign of fraying helix ends often encountered in peptide termini. In SDS micelles (Figure 3A, right), several α-helix NOE connectivities are missing in this 5−25 segment when compared to those observed in TFE, especially between Glu15 and Leu20. Moreover, cross-peaks between Lys14 and Leu20 display lower intensities, suggesting differences in the dynamic behavior in this region (see H−D exchange results below). In summary, with regard to medium-range connectivities in SDS micelles, segment 5−18 displays the most typical α-helix ones while that observed in segment 21−25 suggests a flexible helix turn. Due to the lack of NOE

information, the helical status of segment 19−20 remains unclear. Finally, the N-terminal end of the peptide is devoid of medium-range NOEs, and the C-terminal end has only a few medium-range connectivities, indicating a large flexibility at each peptide extremity.

The differences in ^{1}Hα and ^{13}Cα chemical shifts from those found in random coil peptides are additional indicators of the secondary structure (*27*, *28*). Chemical shift differences for ^{1}Hα and ^{13}Cα are shown in panels B and C of Figure 3 for TFE and SDS, left and right, respectively. The long series of negative ^{1}Hα (Δ^{1}Hα < −0.1 ppm) and positive ^{13}Cα chemical shift differences (Δ^{13}Cα > 0.7 ppm) observed in segment 5−25 are typical of an α-helical conformation. However, the smaller Δ^{1}Hα difference for residues Arg18 and Gly19 in both 50% TFE and SDS micelles suggests some flexibility of the α-helix around these residues. In addition, the weaker Δ^{1}Hα and Δ^{13}Cα differences observed for residues 15−19 in SDS micelles suggest that this region is more dynamic than in 50% TFE. These observations are reinforced by proton−deuterium exchange data in SDS showing that segments 13−19 and 21−22 exhibit high H−D exchange rates, indicating a larger solvent accessibility and flexibility when compared to those of the rest of the helix region (Figure 3A, right, ○ and ●, respectively).

Taken together, these results show that in both 50% TFE and SDS micelles, the main body of the peptide adopts an α-helix conformation, including residues 5−25, with some flexibility around residue Gly19. This flexibility appears to be greater in SDS than in 50% TFE, especially for the C-terminal part of the helix (i.e., segment 15−25).

NMR Structure Model of NS5A[1−28]. The numbers of NOE-derived interproton distance constraints used for the structure calculations are reported in Table 1 of the Supporting Information. From the 50 initial computed structures, final sets of 31 and nine low-energy structures were retained for the peptide in 50% TFE and SDS micelles, respectively. Structure selection was based on NOE violations lower than 0.5 Å, and both sets of structures fully satisfied the corresponding experimental NMR data. The final statistics are listed in Table 1 of the Supporting Information.

The superimposition of the 31 calculated structures obtained in 50% TFE is shown in Figure 4A. All structures exhibit a regular α-helical conformation extending from residues Val5 and Leu25, as also reflected by the low local rmsd for the backbone heavy atoms (Figure 3D, left) as well as the low global rmsd of 0.54 Å in this segment.

In contrast, the higher rmsd value of 2.38 Å between residues 5 and 25 for the set of nine structures in SDS micelles reflects an apparent conformational heterogeneity. This is highlighted in the superimposition of the nine structures (Figure 4C) showing some conformational fluctuations of the backbone around residue Gly19. However, each helical segment (5−19 and 19−25) is well defined, as indicated by their lower global rmsds of 0.73 and 0.93, respectively (see the Supporting Information). The local conformational fluctuations around Gly19 are illustrated by the high local rmsd values, including residues 17−21, when compared to the low values of ∼0.1 Å observed in well-defined regions (Figure 3D, right). In addition, due to the presence of noncanonical dihedral angles and low helix backbone H-bond energies, region 17−22 is assigned as either α-helical or coiled when the set of nine calculated

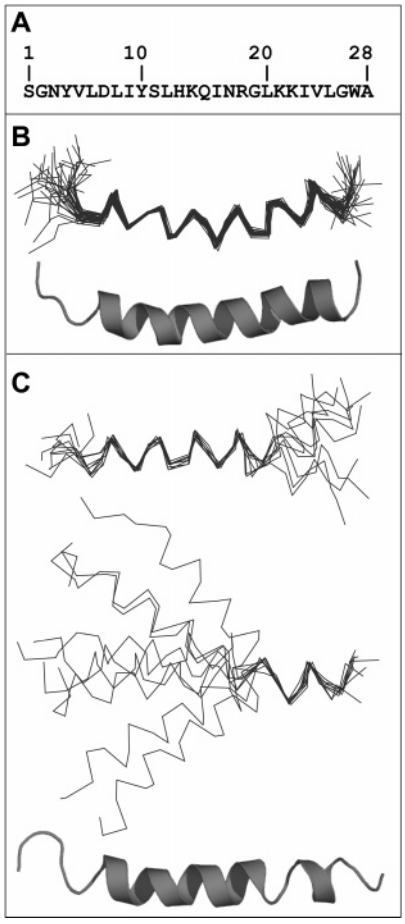

FIGURE 4: Structural characterization of the BVDV NS5A[1−28] peptide. (A) Peptide sequence. (B) Superimposition of the backbone heavy atoms (N, Cα, and C′) of the 31 final structures in 50% TFE (top, PDB entry 2AJJ) and a cartoon representation of the average structure (bottom, PDB entry 2AJN). The 31 structures were superimposed for the best overlap of residues 5−25, corresponding to the α-helical segment. (C) Superimposition of the final set of nine structures in 100 mM SDS (top and middle, PDB entry 2AJM) and a cartoon representation of a representative structure selected from the nine final structures (bottom, PDB entry 2AJO). The nine structures were superimposed for the best overlap of either residues 5−19 (top) or 19−25 (middle), which correspond to the well-defined α-helical segments.

structures in SDS is analyzed by VADAR (*43*). This is illustrated in the representative structure reported in Figure 4C (bottom). These conformational fluctuations are in agreement with the various NMR data reported above in this region (low Hα and Cα chemical shift differences, high H−D exchange rate, low intensities of medium-range NOEs, α_i−β_{i+3} connectivities) and suggest that residues surrounding Gly19 constitute an intrinsic flexible helical element of the BVDV NS5A[1−28] membrane anchor. This flexibility was further documented by molecular dynamic simulation (see below). Finally, both edges of the 5−25 α-helix in TFE and SDS (panels B and C of Figure 4, respectively) appeared to be unstructured. However, these apparent structural instabilities might be explained by the absence of stabilizing interactions with the rest of NS5A and/or membrane phospholipids in the context of the isolated NS54[1−28] peptide.

Despite the local conformation differences observed between the NS5A[1−28] structures in 50% TFE and SDS micelles, the asymmetric distribution of polar and hydrophobic residues on each side of helix 5−25 clearly reveals

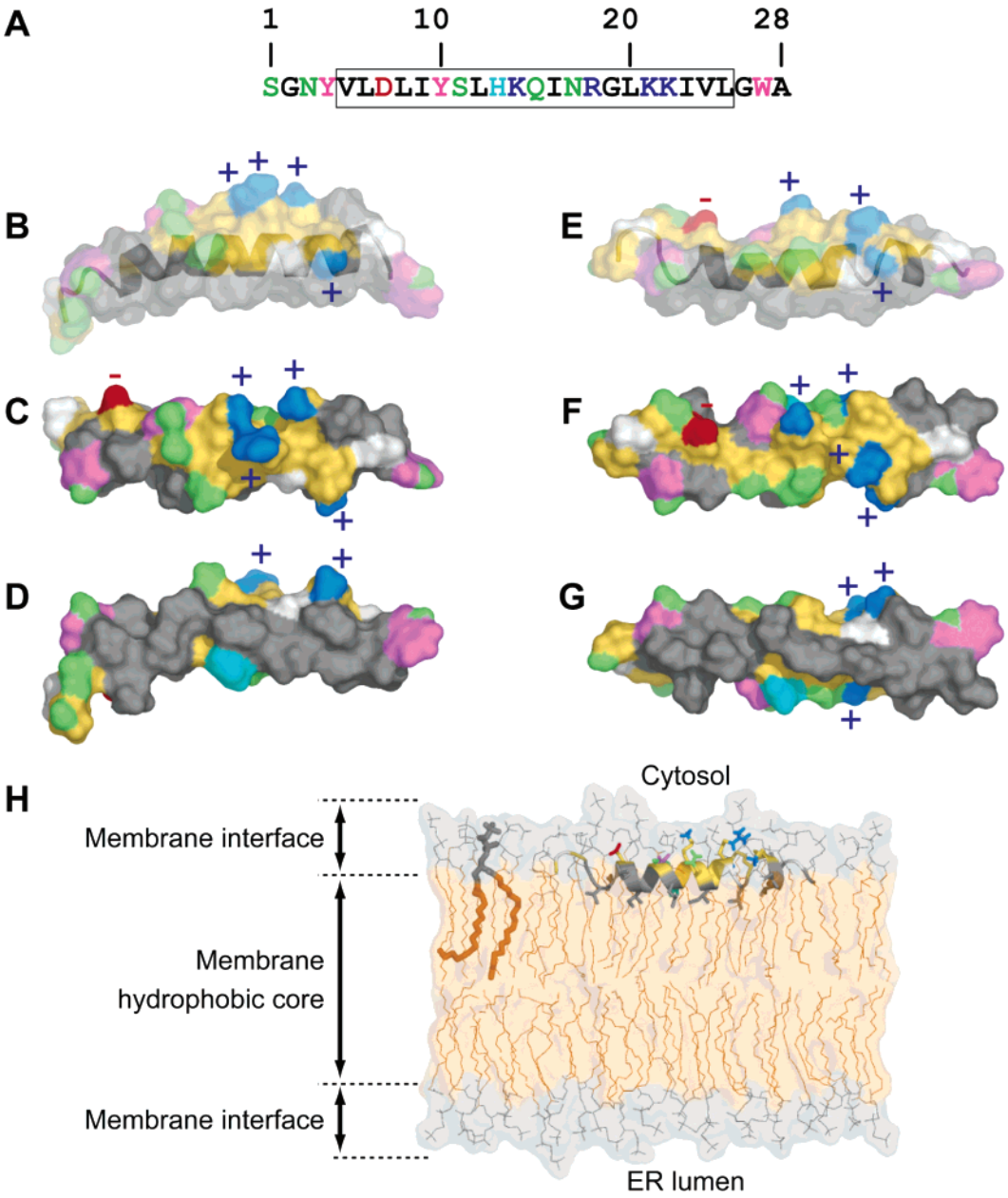

FIGURE 5: Structures of the NS5A aa 5−25 amphipathic α-helix in 50% TFE (left) and 100 mM SDS (right) and expected location in the membrane. (A) The aa sequence of NS5A[1−28], including helix 5−25 (box). (B−D) Side, top, and bottom views of the surface of the NS5A[1−28] average structure in 50% TFE (PDB entry 2AJN). (E−G) Side, top, and bottom views of the surface of a NS5A[1−28] representative structure in 100 mM SDS (PDB entry 2AJO). The structure backbones are displayed as ribbons in panels B and E. Residues are color-coded according to their physicochemical properties. Hydrophobic (A, V, L, and I) and polar residues (S, N, D, Q, H, K, and R) are colored gray and yellow, respectively, except for Trp and Tyr (magenta) and Gly (white). Positively and negatively charged groups of basic (K and R) and acidic (D and E) residues are colored blue and red, respectively. Hydrophilic neutral groups (OH, NH, and CO) of polar residue side chains (S, N, Q, Y, and W) are colored green, and the histidine ring is colored cyan. The aa sequence of NS5A[1−28] is colored accordingly (A). (G) Expected location and orientation of the BVDV NS5A amphipathic α-helix in the membrane. The positioning of the peptide backbone (ribbon representation) and residue side chains (stick representation) at the interface between polar heads and hydrophobic tails of phospholipids was deduced from the molecular dynamics simulations in water and dodecane reported in Figure 6. The simulated model of the POPC bilayer was obtained from refs *18* and *19* (http://moose.bio.ucalgary.ca/). A single POPC molecule in a thick stick representation is shown at the right. The polar head and the hydrophobic tail of phospholipids are colored light gray and orange, respectively. Panels B−H were rendered with the PyMOL molecular graphics system (DeLano Scientific, http://www.pymol.org).

the amphipathic character of this α-helix (Figure 5B−G). However, the positioning of residues along helix 5−25 in 50% TFE defines slightly twisted hydrophobic and hydrophilic grooves (Figure 5B−D). This is due to the slight bending of the helix determined in 50% TFE. Such bending often observed for isolated helices in TFE studied by NMR is mainly due to the lack of long-range distance restraints when the 3D structure is calculated. In contrast, both hydrophilic and hydrophobic grooves are clearly more linear for the structure determined in SDS micelles (Figure 5E−G). This structural feature might be explained by the flexible region centered on Gly19 which possibly allows the peptide to adapt to the water−SDS micelle interface. As illustrated in Figure 5F for the structure determined in SDS, all charged and polar chemical groups of residues are exposed along both edges of the hydrophilic side of the peptide. On the other

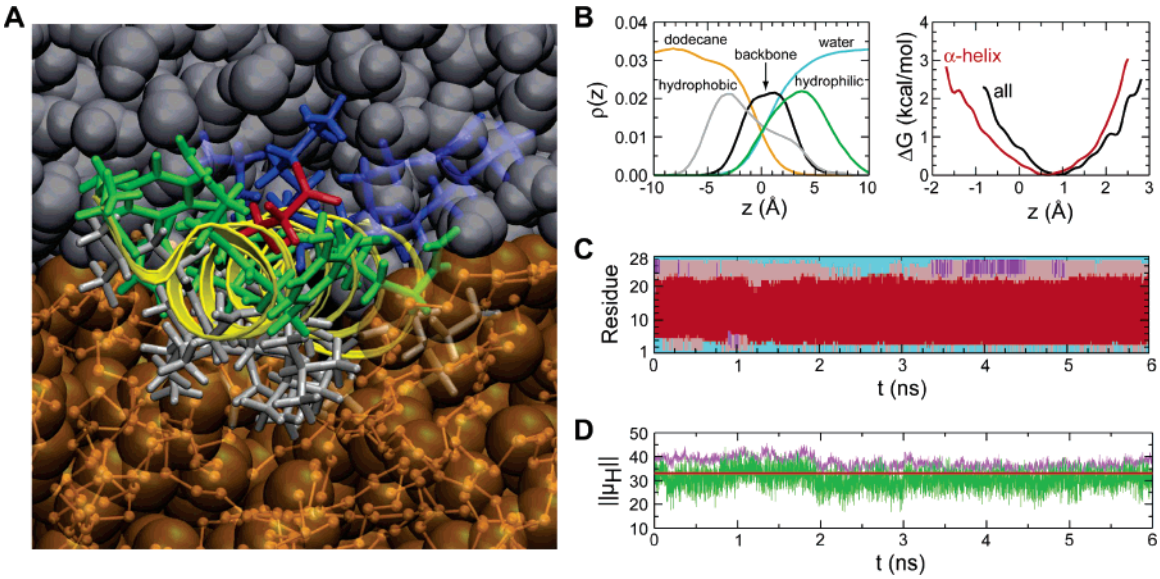

FIGURE 6: Analysis of the NS5A[1−28] molecular dynamics at a water−dodecane interface. (A) Snapshot of the assayed peptide at the water−dodecane interface at 6 ns. The backbone is depicted as a yellow ribbon. Hydrophobic, hydrophilic, negatively charged, and positively charged side chains are colored gray, green, red, and blue, respectively. The reader is looking down the helix from its N-terminus. Water and dodecane molecules are represented as van der Waals spheres colored light blue and orange, respectively. Dodecane chains are also represented as sticks. (B) Density profiles (left) and free energy profiles (right) describing the position of the assayed peptide with respect to the water−dodecane interface. In density profiles, water is colored cyan, dodecane orange, and the peptide backbone green and hydrophobic and hydrophilic side chains are colored black and blue, respectively. The free energy profile of all backbone atoms is colored black, while that of α-helix is colored red. For clarity, the origin of the *z*-axis has been set at the interface (in fact, the interface was located 17.8 Å from the dodecane center of mass). (C) Secondary structure evolution of the assayed peptide during the molecular dynamics simulation. The secondary structure is computed in eight states by Stride (*35*); the α-helical content is shown in red, the 3_{10}-helix content in purple, the turn content in pink, and the coil content in cyan. (D) Hydrophobic moment of the assayed peptide during the simulation colored purple. The red line is the hydrophobic moment computed for the whole peptide constraints as canonical α-helix and residue side chain orientation. The green curve is the hydrophobic moment of this canonical helix but with the side chain orientation of the assayed peptide during the dynamics (the canonical α-helix was fitted on the backbone of the assayed peptide during the dynamics).

hand, aromatic rings of Tyr4 and Trp27 appear to be well positioned at the hydrophilic−hydrophobic interface, suggesting an essential role in the membrane association of the peptide. A similar role could be assigned to Tyr10, although it appears mainly located on the hydrophilic helix side.

Positioning of NS5A[1−28] in SDS Micelles. The positioning of the peptide in SDS micelles was investigated by assessing the proton−deuterium exchange of the amide proton by NMR using either lyophilized protonated peptide/SDS micelles dissolved in D_2O or lyophilized amide-deuterated peptide/SDS micelles dissolved in H_2O. The disappearance or appearance of amide protons was estimated on the basis of NOESY spectra recorded at various time points up to the exchange of all amide protons (72 h). These analyses allowed us to distinguish four groups of exchangeable amide protons: rapid exchange (less than 3 h), residues 1−3, 15, 17, and 28; intermediate exchange (from 3 to 6 h), residues 4, 13, 14, 16, 26, and 27; slow exchange (from 6 to 14 h), residues 7, 18, 19, 21, and 22; very slow exchange (>14 h), residues 5, 6, 8−12, 20, 23, and 24 (the latter are reported with filled circles in Figure 3A, right). All hydrophobic residues but Ile16 belonging to helical region 5−25 appeared to be slowly exchangeable, indicating that they are likely buried in the SDS micelle hydrophobic core. In contrast, most of the hydrophilic residues are rapidly exchangeable and thus likely exposed at the micelle surface. These data indicate that amphipathic helix 5−25 is located at the SDS micelle surface with its hydrophobic side interacting with the hydrophobic core of the micelle. Interestingly, two distinct regions connected by the 13−17 polar helical element emerge from these analyses. The N-terminal portion (residues 5−12), including polar residues Asp7 and Ser11 exhibiting slowly exchangeable amide protons, appears to be very hydrophobic. This region, which forms a very stable α-helix in SDS according to the medium-range NOE connectivities (Figure 3A, right), is likely more buried in the micelle core than the basic C-terminal helix of residues 18−25. From these data, it is possible to deduce that amphipathic helix 5−25 forms an in-plane amphipathic α-helix embedded at the phopholipid interface in the membrane context.

Molecular Dynamics of BVDV NS5A[1−28] at a Water−Dodecane Interface. To investigate further the positioning of NS5A segment 1−28 in a membrane as well as its putative conformational fluctuations reported above, we studied the behavior of the peptide structure by MD simulations at a water−oil interface utilized to mimic the hydrophilic−hydrophobic interface of a water−membrane arrangement (*37*, *44*, *45*). For the simulations, the average structure determined in 50% TFE was chosen (PDB entry 2AJN) because of the homogeneity of the set of calculated structures in this medium. In the equilibration step, stabilization of temperature and energy was reached in less than 6 ps, and they became remarkably stable after that period. The water−dodecane interface remains stable, and marginal water diffusion in the hydrophobic phase was observed. The optimal positioning of the peptide at this interface was, however, significantly longer and occurs over ca. 1 ns. The production step was thus run over 6 ns (Figure 6). A snapshot of the system at the end of the simulation is reported in

Figure 6A**,** and an animated video of the 6 ns molecular dynamics simulation is available as Supporting Information. During the entire production period, the NS5A[1−28] peptide remained at the water−dodecane interface (see Figure 1 of the Supporting Information). The average distance between the centers of mass of the peptide and the dodecane lamella was 18.6 ± 0.6 Å over the 6 ns. The total displacement of the peptide along the normal (i.e., *z*-axis) to the interface plane was 4.2 Å in the course of the equilibration and production steps. During the latter period, the peptide diffused freely in the plane of the water−dodecane interface.

The water−dodecane interface can be visualized in the atom density profiles (Figure 6B, left) and is located where the density profiles of water (cyan line) and dodecane (orange line) intersect (origin of the *z*-axis). The free energy profile reported in Figure 6B (right, black line) shows that the peptide center of mass was located at ∼0.8 Å above the interface, on the water phase. As shown by the increase in ΔG, a significant energetic penalty was witnessed when the peptide moved from this equilibrium position. The density profiles (Figure 6B, left) show that the peptide backbone atoms appear to gather preferentially in the water phase. In fact, the backbone density curve results from the additive contribution of helical segment 5−25 and nonhelical segments 1−4 and 26−28. When examined independently, the backbone of the helical segment is closer to the water−dodecane interface (∼0.6 Å above), albeit still in the aqueous phase (Figure 6B, right, red line). As expected, the density profile shows that the hydrophilic side chains were exposed to the water medium (Figure 6B, left). Interestingly, the time-average density of basic (Arg18 and Lys14, -21, and -22) and acidic (Asp7) side chains does not seem to be directly correlated with their length. Indeed, the density profile of Asp7 is close to that of Arg18 or Lys21 (Figure 2A of the Supporting Information). Although the hydrophobic side chains were essentially buried in the dodecane phase, a bimodal density profile was observed (Figure 6B, left). This is mainly due to Leu6 and Ala28 exposed to the aqueous environment, while all other aliphatic side chains are clearly oriented toward the dodecane phase (for details, see Figure 2B of the Supporting Information). Aromatic residues Tyr4 and Trp27 as well as His13 are the residues closest to the interface (Figure 2C of the Supporting Information). In summary, the segregation of residue side chains between the water and dodecane phase is consistent with the periodicity of hydrophilic and hydrophobic residues in the α-helical conformation.

The evolution of NS5A[1−28] secondary structure during the simulation shows that the regular α-helical conformation extending from residue 5 to 25 in the initial peptide structure in 50% TFE was slightly modified at both ends of the helix (Figure 6C). At the N-terminus, the α-helix extended to residue 3 during the first 1.4 ns of simulation and then remained stable. At the C-terminus, the α-helix initially extending to residue 25 tends to stop at residue 23, while residues from position 24 to 27 were assigned as a turn conformation and transiently as a 3_{10}-helix. In fact, segment 22−26 tends to globally adopt a noncanonical α-helical conformation, as denoted by the average values of torsion angle ϕ which were smaller than the canonical value in the α-helix. This corresponds to the last visible turn of the helix in Figure 6A, which appears to be larger than in the α-helix.

These conformational changes can be seen as the adaptation of the peptide to the water−dodecane interface. A measurement of this adaptation is given by the values of the first-order hydrophobic moment, μ_H (*33*), which include both the peptide backbone conformation and the side chain orientations (Figure 6D). First, the hydrophobic moment of the assayed peptide was roughly oriented perpendicular to the dodecane phase, and its *z* coordinate was relatively stable. Second, the norm of μ_H was systematically larger in the assayed peptide (purple curve) than for a theoretical peptide with a canonical α-helix and either a perpendicular orientation of residue side chains (red line) or the orientation of side chains of the assayed peptide during the dynamics (green curve). In the latter case, the canonical α-helix was fitted to the backbone of the assayed peptide at each time point during the dynamics. The conformational changes reported above at the C-terminus of the peptide during the simulation and affecting the orientation of the side chains allow the peptide to exhibit a larger hydrophobic moment than would be observed for a canonical α-helix, or for the peptide structure in 50% TFE.

Interestingly, the structure of the peptide at the end of the simulation appears to be closer to the NMR structures obtained in the presence of SDS micelles than to the average structure obtained in 50% TFE, whereas the latter has been used as the initial structure for the simulation. Typically, the groove of hydrophobic residues is linear in both SDS and MD structures while it is twisted for the structure in 50% TFE. As TFE stabilizes helices by strengthening their hydrogen bonds (*46*), it tends to yield rigid α-helices as observed here for helix 5−25. The twisted hydrophobic groove observed in the structure thus appears as a consequence of the rigidity of helix 5−25 in 50% TFE. Importantly, the untwisting of this hydrophobic groove observed during the MD simulation supports the presence of the flexible region revealed by the NMR structure analysis in SDS. In addition, the histogram of the local rmsd evaluated over the 6 ns of MD production reveals a slightly higher rmsd for region 19−21 than for the surrounding regions (see Figure 2 of the Supporting Information). Although these data are consistent with the flexibility of the backbone around residue Gly19, it remains very limited. This could, however, be due to the difference in the time scales being explored by MD simulations and NMR simulations (i.e., a few nanoseconds and hundreds of milliseconds, respectively). Finally, it is worth noting that both MD simulations and NMR data clearly show that the N-terminal half of helix 5−25 is the most stable region of the membrane anchor.

From the combination of both NMR and MD simulation results, it is possible to propose a reasonable positioning of the NS5A[1−28] structure in a model membrane (Figure 5H) with the helix backbone located at the boundary between the alkyl chains and the polar headgroups, i.e., at the level of the glycerol groups of phospholipids. This positioning is similar to that we deduced from the NMR analysis of the HCV NS5A[1−31] membrane anchor in SDS and DPC micelles (*11*).

Comparison of BVDV NS5A[1−28] and HCV NS5A[1−31] Sequences. Although there are no obvious aa sequence similarities between BVDV and HCV NS5A membrane anchors, the experimental demonstration of the presence of a long amphipathic α-helix for both proteins (this study and

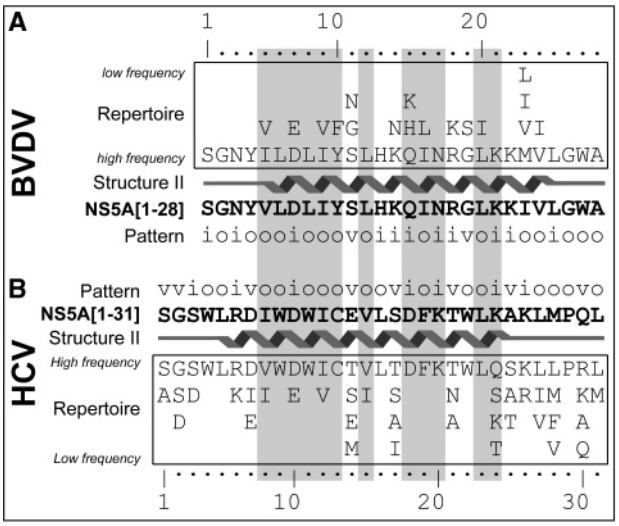

FIGURE 7: Comparison of BVDV NS5A[1−28] and HCV NS5A-[1−31] membrane anchor sequences. (A) BVDV[1−28] sequence (EMBL accession number M31182) and HCV NS5A[1−31] sequence (EMBL accession number M67463) are reported as reference sequences and numbering for BVDV and HCV, respectively (middle). The experimentally determined α-helices (residues 5−25) of NS5A from BVDV (this study) and HCV (*13*) are schematically reported above and under each reference sequence, respectively. The aa repertoires at each sequence position for BVDV NS5A[1−28] (top) and for HCV NS5A[1−31] (bottom) segments were deduced from the multiple alignment of sequences retrieved using the BLAST homology search program. Sets of 16 and 107 sequences were considered for the BVDV NS5A[1−28] and HCV NS5A[1−31] repertoires, respectively. The amino acids are listed in decreasing order of observed frequency, from bottom to top for BVDV NS5A[1−28] and from top to bottom for the HCV NS5A-[1−31] segment. Only residues observed more than twice at a given position were considered. Hydropathic consensus patterns were deduced from the corresponding repertoires: (i) hydrophilic positions (including T, S, K, Q, N, H, E, D, and R), (o) hydrophobic positions (including F, I, W, Y, L, V, M, P, C, A, and G), and (v) variable positions (i.e., where either hydrophilic or hydrophobic residues were observed). Identical hydrophobic or hydrophilic positions within BVDV and HCV helices are highlighted in light gray.

ref *11*) led us to compare their sequences to better define the structural determinants of in-plane amphipathic membrane helices. To facilitate the comparison of the numerous NS5A N-terminal sequences from HCV and BVDV variants reported in generic databases, the repertoires of aa at each sequence position were deduced from multiple alignments (Figure 7). Amino acids were listed in decreasing order of observed frequency, from bottom to top for BVDV NS5A-[1−28] and from top to bottom for HCV NS5A[1−31]. These repertoires show that (i) numerous residues are conserved at specific positions, (ii) most of the other positions showing apparent variability are occupied by residues with similar hydropathic character, i.e., either hydrophilic (i) or hydrophobic (o), and (iii) only a few positions appear to be variable (v), i.e., when either hydrophilic or hydrophobic was observed. The letter-coded motifs summarizing the deduced hydropathic patterns of BVDV NS5A[1−28] and HCV NS5A[1−31] are shown in the middle of Figure 7. The comparison of these patterns shows that most of the aligned positions in the helices exhibit the same hydropathic character (highlighted in light gray in Figure 7). In addition, the corresponding hydrophobic and hydrophilic positions are located at regular intervals in the sequences, in agreement with the amphipathic nature of these helices. The main differences between the BVDV and HCV repertoires appear to be the number and the repartition of aromatic and charged residues along the sequences (see the Discussion). Of particular interest is an acidic position in the first part of the sequences that is highly conserved in BVDV and HCV (positions 7 and 10, respectively). Both positions $i - 1$ and $i + 1$ of acidic position i exhibit fully conserved Trp residues in HCV, while fully conserved Leu residues are observed in BVDV. Interestingly, for both viruses, positions $i - 2$ and $i + 2$ are occupied by β-branched hydrophobic residues (i.e., either Ile or Val). Hence, this small symmetric segment of five aa can be considered as a canonical amphipathic helix−turn motif, i.e., β-branched hydrophobic residues (Trp or Leu)−acidic residue−(Trp or Leu)−β-branched hydrophobic residues. In both BVDV and HCV membrane anchor structures, this motif belongs to the most stable and hydrophobic part of the amphipathic helix, indicating that it likely plays a crucial role for membrane anchoring. It possibly constitutes a typical motif of an in-plane amphipathic membrane helix, at least for the NS5A proteins in genera *Hepacivirus* and *Pestivirus*. To sum up, BVDV and HCV membrane anchors exhibit a similar structural organization despite a low degree of sequence similarity.

DISCUSSION

Three-dimensional NMR structure analyses of the BVDV NS5A[1−28] peptide performed either in 50% TFE or in SDS micelles to mimic the membrane environment revealed that the N-terminal membrane anchor of NS5A includes a long amphipathic α-helix (aa 5−25) divided into two portions separated by a flexible region centered around residue Gly19. The proton−deuterium exchange NMR analysis in SDS micelles showed that the helix hydrophobic residues were mainly buried in the hydrophobic core of the detergent/peptide micelles, whereas the polar and charged aa were mainly accessible at their surface. By MD simulation at a water−dodecane interface to mimic the hydrophobic−hydrophilic interface of phospholipids in a membrane, the peptide helix backbone was found to be located at the interface with the hydrophobic aa mainly buried in the dodecane, whereas the polar and charged aa were found in the water phase. It can thus be concluded that the BVDV NS5A membrane anchor is embedded in-plane in the cytosolic leaflet of the membrane by an amphipathic helix exhibiting a hydrophobic side buried in the membrane and a polar/charged side accessible from the cytosol.

The MD simulation of NS5A[1−28] in a water−dodecane environment is assumed to reflect the behavior of the peptide at the hydrophobic−hydrophilic interface of membrane phospholipids. The average structure of the peptide in 50% TFE used for simulation tends to be quickly stabilized at the water−dodecane interface, but a noteworthy mobility is preserved. The conformation of both ends of the helix evolved toward a longer α-helix at the N-terminus and a globally helical but noncanonical α-helix at the C-terminus. Concurrently, the twisted hydrophobic groove observed in the structure in 50% TFE rapidly evolved to yield a straight hydrophobic groove similar to that observed in the structure determined in SDS micelles. This conformation is the most favorable for the interaction of the hydrophobic residues with the planar dodecane phase. These conformational changes

correspond to the structural adaptation of the peptide backbone and side chains to the hydrophobic interface of dodecane and seem to be due to the flexibility of the C-terminal region of the helix. It is thus tempting to conclude that the dynamical behavior of this region should allow the peptide to adapt to the hydrophilic−hydrophobic interface of the phospholipid layer. Interestingly, our previous structural analysis of NS5A[1−31] from HCV (*11*, *13*) has pointed out a potential flexible region centered on Leu16 in the α-helix which might play a similar adaptation role. It is thus possible that such a flexible element constitutes a particular structural feature of in-plane amphipathic membrane helices for their adaptation to the membrane interface.

The MD simulation also shows that the backbone of the helical segment spans the water−dodecane interface, in contrast with segments outside the helix which are preferentially exposed to the water phase. In the context of a phospholipid membrane, the peptide is expected to be located at the boundary between the alkyl chains and the polar headgroups, as previously observed in MD simulations of melittin, a well-studied in-plane membrane amphipathic peptide (*47*). The schematic view of the putative position of NS5A[1−28] in a phospholipid bilayer (Figure 5H) illustrates this feature, with the backbone of NS5A[1−28] located at the level of the glycerol group of phospholipids. This particular location renders the polar side of this helix accessible at the membrane surface. The presence of four basic residues (Lys and Arg) in the polar side of α-helix 5−25 is in keeping with the high frequency of these residues in helices at the membrane−water interface region in transmembrane and monotopic membrane proteins (*17*). Intriguingly, these residues are essentially located in the C-terminal half of the helix, forming a cluster of positive charges. In contrast, the single acidic residue is located in the highly hydrophobic, N-terminal part of the helix (Asp7). These charged groups, together with the polar groups of the other hydrophilic residues present in the polar helix side, exhibit a particular arrangement at the peptide surface (shown in Figure 5F). The resulting motif likely forms a specific interaction site that could mediate specific protein−protein interactions at the membrane surface as already proposed for the NS5A amphipathic helix from HCV (*11*, *13*).

In membrane proteins, Trp is known to be preferentially located at the membrane interface (*48*, *49*) and its presence at the interface between the hydrophilic and hydrophobic sides of in-plane amphipathic membrane helices is a typical feature. For example, the HCV NS5A membrane anchor (*11*, *13*) and the membrane-proximal region of human immunodeficiency virus glycoprotein gp41 (*50*) include four and five Trp residues, respectively. In contrast, only one Trp residue is present in the BVDV NS5A N-terminal sequence, but outside of the experimentally determined α-helix (Trp27). Examination of the BVDV NS5A[1−28] structure suggests that Tyr4 located at the hydrophilic−hydrophobic interface likely plays a similar role. In contrast, the reason for the involvement of Tyr10 is unclear as it is mainly in the water phase. Indeed, a recent statistical study of aa in helices at membrane−water interface regions in transmembrane and monotopic membrane proteins reported that Tyr and Trp are very frequently found at the membrane interface and that most side chains of these residues are directed toward the membrane (*17*). This is in keeping with our observation during MD simulation which showed that Trp and Tyr side chains were located at the water−dodecane interface. This feature further points out the role of these residues as membrane anchors. Besides, among the hydrophobic residues, Leu seems to be a particularly important residue for membrane anchorage as it represents 21% of the residues observed in the interface regions of monotopic proteins (*17*). As many as five Leu residues are present in BVDV NS5A helix 5−25, four of them being fully conserved among the 17 sequences of BVDV variants reported (Leu6, -8, -12, and -25) and the fifth Leu (Leu20) being substituted with Ile in some variant (see the BVDV aa repertoire in Figure 7). In addition, Ile at position 16 can also be substituted with a Leu in some variants, pointing out a similar role of Ile in membrane anchorage. In summary, although the Trp residue is poorly represented in the BVDV NS5A membrane anchor, helix 5−25 exhibits a sufficient number of membrane anchor residues (Tyr, Leu, and Ile) to ensure the anchoring of this amphipathic helix to the hydrophobic core of the phospholipid bilayer.

The phylogenetic proximity between HCV and BVDV suggests a similar role for their NS5A proteins. Moreover, examination of the BVDV NS5A aa sequence downstream of the N-terminal membrane anchor using various bioinformatics tools suggests an organization in three domains similar to that reported for NS5A of HCV (*2*). In addition, multiple alignments of NS5A domain I from HCV and related viruses indicate the putative conservation of a zinc binding motif (*14*). These features suggest that the N-terminal helix anchor of BVDV NS5A should exhibit the same structure−function relationships as its HCV counterpart. From the structural point of view, the comparative NMR structure analyses of HCV NS5A[1−31] (*11*, *13*) and BVDV NS5A[1−28] (this study) reveal the presence of a common long amphipathic helix of 26 residues exhibiting a common hydropathic pattern (see Figure 7) and including a putative local flexible region. For both proteins, the N-terminal part of this helix appears to be very stable and hydrophobic and includes a similar amphipathic helix−turn motif that likely plays a crucial role in membrane anchoring, while the C-terminal part of the helix appears to be more hydrophilic and basic. These features suggest a major role in membrane anchoring for the former, while the latter might be more important in mediating intermolecular interactions. Finally, the local flexibility in both helices might be required to ensure the most favorable interactions of the helix residue side chains with their respective hydrophilic and hydrophobic sides at the polar headgroup−alkyl chain interface of the phospholipid layer. Alternatively or additionally, this flexible region might play a role in the folding of the helix at the membrane interface.

It is noteworthy that the NMR structure analysis of the membrane-binding C-terminus of bovine milk component PP3 revealed the presence of a bend dividing this long 38-residue helical region into two amphipathic α-helical segments, both residing in the plane of the bilayer (*51*). In a manner similar to what we observed for the NS5A membrane anchor, this bend is likely a means of ensuring the most favorable contacts between lipid hydrocarbons and the hydrophobic regions of the peptide (*51*). With regard to the few monotopic membrane proteins of known 3D structure available to date, all of them have short amphipathic α-helices residing in the plane of the membrane-binding

interface. Prostaglandin H synthase isoforms 1 and 2 bind to the ER membrane via four short in-plane amphipathic α-helices that form a horseshoe-shaped planar motif and interact with one leaflet of the phospholipid bilayer (*52*, *53*). The membrane anchoring region of squalene cyclase forms a flat nonpolar plateau consisting of one amphipathic α-helix, one loop, and one segment between two helices (*54*). Fatty acid amide hydrolase (*55*) and monoamine oxidase B (*56*) both contain one predicted transmembrane helix but also exhibit a membrane interacting domain that includes two amphipathic α-helices and one short hydrophobic loop, respectively. In contrast to NS5A proteins, these various in-plane membrane amphipathic α-helices are relatively short (one to four helix turns), suggesting that they could bind at the membrane interface without causing a major conformational change. Interestingly, molecular dynamics simulation performed on the membrane anchoring domain of prostaglandin H synthase revealed that helices A−C undergo rigid-body motions upon binding to a membrane interface (*18*). These motions, arising from the flexibility of the interhelical loops, are in keeping with the membrane interface adaptation of the long amphipathic α-helices of NS5A or PP3 proteins due to the presence of an internal flexible region. Taken together, these various observations suggest that internal helix flexibility and/or flexible interhelical loops are a common feature of in-plane membrane anchors of monotopic membrane proteins, ensuring the most favorable polypeptide chain adaptation to the specific physicochemical environment of the membrane interface.

It should be emphasized that the few monotopic membrane proteins of known structure exhibit enzymatic activities on lipid-soluble substrates, some of them involving an intimate relationship between the membrane-binding surface and the active site (*52*−*55*). The function of NS5A is as yet unknown. The HCV NS5A membrane-anchoring helix has been assumed to interact at least in part with the rest of the protein (*11*, *13*) but possibly not with domain 1 (*14*). To date, there is however no experimental evidence supporting these hypotheses. Nevertheless, our recent mutational analyses (*11*, *13*) concluded that the HCV NS5A-anchoring helix constitutes a unique platform that is likely involved in specific interactions essential for the assembly of the HCV replication complex. A similar role is expected for the NS5A-anchoring helix of BVDV and is supported by the common structural features of these helices. The targets of the putative membrane surface interaction sites defined by HCV or BVDV helix anchors remain to be determined.

ACKNOWLEDGMENT

We gratefully acknowledge D. Ficheux for the peptide synthesis, Dr. F. Dorkeld for the availability of the repertoire program, and Drs. C. Combet and C. Geourjon for NPSA and euHCVdb facilities.

SUPPORTING INFORMATION AVAILABLE

One table containing the statistics of the simulated annealing structures of BVDV NS5A[1−28] in 50% TFE and 100 mM SDS, two figures containing various analyses of molecular dynamics simulation data (backbone and side chain positions and detailed energy profiles of residues with respect to the water−dodecane interface; local rmsd of the peptide structure), and an animated movie of the 6 ns molecular dynamics simulation. This material is available free of charge via the Internet at http://pubs.acs.org.

REFERENCES

1. Reed, K. E., Gorbalenya, A. E., and Rice, C. M. (1998) The NS5A/NS5 proteins of viruses from three genera of the family flaviviridae are phosphorylated by associated serine/threonine kinases, *J. Virol. 72*, 6199−206.
2. Tellinghuisen, T. L., Marcotrigiano, J., Gorbalenya, A. E., and Rice, C. M. (2004) The NS5A protein of hepatitis C virus is a zinc metalloprotein, *J. Biol. Chem. 279*, 48576−87.
3. Neddermann, P., Quintavalle, M., Di Pietro, C., Clementi, A., Cerretani, M., Altamura, S., Bartholomew, L., and De Francesco, R. (2004) Reduction of hepatitis C virus NS5A hyperphosphorylation by selective inhibition of cellular kinases activates viral RNA replication in cell culture, *J. Virol. 78*, 13306−14.
4. Evans, M. J., Rice, C. M., and Goff, S. P. (2004) Phosphorylation of hepatitis C virus nonstructural protein 5A modulates its protein interactions and viral RNA replication, *Proc. Natl. Acad. Sci. U.S.A. 101*, 13038−43.
5. Appel, N., Pietschmann, T., and Bartenschlager, R. (2005) Mutational analysis of hepatitis C virus nonstructural protein 5A: Potential role of differential phosphorylation in RNA replication and identification of a genetically flexible domain, *J. Virol. 79*, 3187−94.
6. Macdonald, A., and Harris, M. (2004) Hepatitis C virus NS5A: Tales of a promiscuous protein, *J. Gen. Virol. 85*, 2485−502.
7. Tellinghuisen, T. L., and Rice, C. M. (2002) Interaction between hepatitis C virus proteins and host cell factors, *Curr. Opin. Microbiol. 5*, 419−27.
8. Tan, S. L., and Katze, M. G. (2001) How hepatitis C virus counteracts the interferon response: The jury is still out on NS5A, *Virology 284*, 1−12.
9. Gosert, R., Egger, D., Lohmann, V., Bartenschlager, R., Blum, H. E., Bienz, K., and Moradpour, D. (2003) Identification of the hepatitis C virus RNA replication complex in Huh-7 cells harboring subgenomic replicons, *J. Virol. 77*, 5487−92.
10. Penin, F., Dubuisson, J., Rey, F. A., Moradpour, D., and Pawlotsky, J. M. (2004) Structural biology of hepatitis C virus, *Hepatology 39*, 5−19.
11. Brass, V., Bieck, E., Montserret, R., Wolk, B., Hellings, J. A., Blum, H. E., Penin, F., and Moradpour, D. (2002) An amino-terminal amphipathic α-helix mediates membrane association of the hepatitis C virus nonstructural protein 5A, *J. Biol. Chem. 277*, 8130−9.
12. Elazar, M., Cheong, K. H., Liu, P., Greenberg, H. B., Rice, C. M., and Glenn, J. S. (2003) Amphipathic helix-dependent localization of NS5A mediates hepatitis C virus RNA replication, *J. Virol. 77*, 6055−61.
13. Penin, F., Brass, V., Appel, N., Ramboarina, S., Montserret, R., Ficheux, D., Blum, H. E., Bartenschlager, R., and Moradpour, D. (2004) Structure and function of the membrane anchor domain of hepatitis C virus nonstructural protein 5A, *J. Biol. Chem. 279*, 40835−43.
14. Tellinghuisen, T. L., Marcotrigiano, J., and Rice, C. M. (2005) Structure of the zinc-binding domain of an essential component of the hepatitis C virus replicase, *Nature 435*, 374−9.
15. Tautz, N., Meyers, G., and Thiel, H. J. (1998) Pathogenesis of mucosal disease, a deadly disease of cattle caused by a pestivirus, *Clin. Diagn. Virol. 10*, 121−7.
16. Lindenbach, B. D., and Rice, C. M. (2001) Flaviviridae: The viruses and their replication, in *Fields virology* (Knipe, D. M., and Howley, P. M., Eds.) pp 991−1042, Lippincott Williams & Wilkins, Philadelphia.
17. Granseth, E., von Heijne, G., and Elofsson, A. (2005) A study of the membrane-water interface region of membrane proteins, *J. Mol. Biol. 346*, 377−85.
18. Nina, M., Berneche, S., and Roux, B. (2000) Anchoring of a monotopic membrane protein: The binding of prostaglandin H2 synthase-1 to the surface of a phospholipid bilayer, *Eur. Biophys. J. 29*, 439−54.
19. Shepherd, C. M., Vogel, H. J., and Tieleman, D. P. (2003) Interactions of the designed antimicrobial peptide MB21 and truncated dermaseptin S3 with lipid bilayers: Molecular-dynamics simulations, *Biochem. J. 370*, 233−43.

20. Apweiler, R., Bairoch, A., Wu, C. H., Barker, W. C., Boeckmann, B., Ferro, S., Gasteiger, E., Huang, H., Lopez, R., Magrane, M., Martin, M. J., Natale, D. A., O'Donovan, C., Redaschi, N., and Yeh, L. S. (2004) UniProt: The Universal Protein knowledgebase, *Nucleic Acids Res. 32*, D115−9.
21. Altschul, S. F., Madden, T. L., Schaffer, A. A., Zhang, J., Zhang, Z., Miller, W., and Lipman, D. J. (1997) Gapped BLAST and PSI-BLAST: A new generation of protein database search programs, *Nucleic Acids Res. 25*, 3389−402.
22. Combet, C., Penin, F., Geourjon, C., and Deléage, G. (2004) HCVDB: Hepatitis C Virus Sequences Database, *Appl. Bioinformatics 3*, 237−40.
23. Thompson, J. D., Higgins, D. G., and Gibson, T. J. (1994) CLUSTAL W: Improving the sensitivity of progressive multiple sequence alignment through sequence weighting, position-specific gap penalties and weight matrix choice, *Nucleic Acids Res. 22*, 4673−80.
24. Penin, F., Geourjon, C., Montserret, R., Bockmann, A., Lesage, A., Yang, Y. S., Bonod-Bidaud, C., Cortay, J. C., Negre, D., Cozzone, A. J., and Deléage, G. (1997) Three-dimensional structure of the DNA-binding domain of the fructose repressor from *Escherichia coli* by ^{1}H and ^{15}N NMR, *J. Mol. Biol. 270*, 496−510.
25. Montserret, R., McLeish, M. J., Bockmann, A., Geourjon, C., and Penin, F. (2000) Involvement of electrostatic interactions in the mechanism of peptide folding induced by sodium dodecyl sulfate binding, *Biochemistry 39*, 8362−73.
26. Favier, A., Brutscher, B., Blackledge, M., Galinier, A., Deutscher, J., Penin, F., and Marion, D. (2002) Solution structure and dynamics of Crh, the *Bacillus subtilis* catabolite repression HPr, *J. Mol. Biol. 317*, 131−44.
27. Merutka, G., Dyson, H. J., and Wright, P. E. (1995) "Random coil" ^{1}H chemical shifts obtained as a function of temperature and trifluoroethanol concentration for the peptide series GGXGG. *J. Biomol. NMR 5*, 14−24.
28. Schwarzinger, S., Kroon, G. J., Foss, T. R., Chung, J., Wright, P. E., and Dyson, H. J. (2001) Sequence-dependent correction of random coil NMR chemical shifts, *J. Am. Chem. Soc. 123*, 2970−8.
29. Wuthrich, K. (1987) Nuclear magnetic resonance—from molecules to man, *Q. Rev. Biophys. 19*, 3−5.
30. Schwieters, C. D., Kuszewski, J. J., Tjandra, N., and Clore, G. M. (2003) The Xplor-NIH NMR molecular structure determination package, *J. Magn. Reson. 160*, 65−73.
31. Laskowski, R. A., Rullmannn, J. A., MacArthur, M. W., Kaptein, R., and Thornton, J. M. (1996) AQUA and PROCHECK-NMR: Programs for checking the quality of protein structures solved by NMR, *J. Biomol. NMR 8*, 477−86.
32. Kale, L., Skeel, R., Bhandarkar, M., Brunner, R., Gursoy, A., Krawetz, N., Phillips, J., Shinozaki, A., Varadarajan, K., and Schulten, K. (1999) NAMD2: Greater scalability for parallel molecular dynamics, *J. Comput. Phys. 151*, 283−312.
33. Silverman, B. D. (2001) Hydrophobic moments of protein structures: Spatially profiling the distribution, *Proc. Natl. Acad. Sci. U.S.A. 98*, 4996−5001.
34. Eisenberg, D., Weiss, R. M., and Terwilliger, T. C. (1984) The hydrophobic moment detects periodicity in protein hydrophobicity, *Proc. Natl. Acad. Sci. U.S.A. 81*, 140−4.
35. Frishman, D., and Argos, P. (1995) Knowledge-based protein secondary structure assignment, *Proteins 23*, 566−79.
36. Humphrey, W., Dalke, A., and Schulten, K. (1996) VMD: Visual molecular dynamics, *J. Mol. Graphics 14*, 33−8, 27−8.
37. Bas, D., Dorison-Duval, D., Moreau, S., Bruneau, P., and Chipot, C. (2002) Rational determination of transfer free energies of small drugs across the water−oil interface, *J. Med. Chem. 45*, 151−9.
38. Brooks, B. R., Bruccoleri, R. E., Olafson, B. D., States, D. J., Swaminathan, S., and Karplus, M. (1983) CHARMM: A Program for Macromolecular Energy, Minimization, and Dynamics Calculations, *J. Comput. Chem. 4*, 187−217.
39. MacKerrel, A. D. D., Bashford, M., Bellott, L., Dunbrack, R. J., Evanseck, J., Fried, M. S., Fischer, J., Gao, H., Guo, S., Ha, D., Joseph, L., Kuchnir, K., Kuczera, T., Lau, F. C., Mattos, S., Michnick, T., Ngo, T., Nguyen, D. B., Prodhom, B., Roux, M., Schlenkrich, J., Smith, R., Stote, J., Straub, M., Watanabe, J., Wiorkiewicz-Kuczera, D., Yin, X., and Karplus, M. (1992) Self-consistent parameterization of biomolecules for molecular modeling and condensed phase simulations, *FASEB J. 6*, A143.
40. Cheatham, T., et al. (1995) Molecular Dynamics on Solvated Biomolecular Systems. The Particle Mesh Ewald Method Leads to Stable Trajectories of DNA, RNA and Proteins, *J. Am. Chem. Soc. 117*, 4193−4.
41. Darden, T., York, D., and Pedersen, L. (1993) Particle mesh Ewald: An N.log(N) method for Ewald sums in large systems, *J. Chem. Phys. 98*, 10089−92.
42. Opella, S. J. (1997) NMR and membrane proteins, *Nat. Struct. Biol. 4* (Suppl.), 845−8.
43. Willard, L., Ranjan, A., Zhang, H., Monzavi, H., Boyko, R. F., Sykes, B. D., and Wishart, D. S. (2003) VADAR: A web server for quantitative evaluation of protein structure quality, *Nucleic Acids Res. 31*, 3316−9.
44. Chipot, C., and Pohorille, A. (1998) Folding and translocation of the undecamer of poly-L-leucine across the water-hexane interface. A molecular dynamics study, *J. Am. Chem. Soc. 120*, 11912−24.
45. Nicolas, J. P. (2003) Molecular dynamics simulation of surfactin molecules at the water-hexane interface, *Biophys. J. 85*, 1377−91.
46. Buck, M. (1998) Trifluoroethanol and colleagues: Cosolvents come of age. Recent studies with peptides and proteins, *Q. Rev. Biophys. 31*, 297−355.
47. Berneche, S., Nina, M., and Roux, B. (1998) Molecular dynamics simulation of melittin in a dimyristoylphosphatidylcholine bilayer membrane, *Biophys. J. 75*, 1603−18.
48. Yau, W. M., Wimley, W. C., Gawrisch, K., and White, S. H. (1998) The preference of tryptophan for membrane interfaces, *Biochemistry 37*, 14713−8.
49. Bechinger, B. (1999) The structure, dynamics and orientation of antimicrobial peptides in membranes by multidimensional solid-state NMR spectroscopy, *Biochim. Biophys. Acta 1462*, 157−83.
50. Schibli, D. J., Montelaro, R. C., and Vogel, H. J. (2001) The membrane-proximal tryptophan-rich region of the HIV glycoprotein, gp41, forms a well-defined helix in dodecylphosphocholine micelles, *Biochemistry 40*, 9570−8.
51. Bak, M., Sorensen, M. D., Sorensen, E. S., Rasmussen, L. K., Sorensen, O. W., Petersen, T. E., and Nielsen, N. C. (2000) The structure of the membrane-binding 38 C-terminal residues from bovine PP3 determined by liquid- and solid-state NMR spectroscopy, *Eur. J. Biochem. 267*, 188−99.
52. Picot, D., Loll, P. J., and Garavito, R. M. (1994) The X-ray crystal structure of the membrane protein prostaglandin H2 synthase-1, *Nature 367*, 243−9.
53. Kurumbail, R. G., Stevens, A. M., Gierse, J. K., McDonald, J. J., Stegeman, R. A., Pak, J. Y., Gildehaus, D., Miyashiro, J. M., Penning, T. D., Seibert, K., Isakson, P. C., and Stallings, W. C. (1996) Structural basis for selective inhibition of cyclooxygenase-2 by anti-inflammatory agents, *Nature 384*, 644−8.
54. Wendt, K. U., Lenhart, A., and Schulz, G. E. (1999) The structure of the membrane protein squalene-hopene cyclase at 2.0 Å resolution, *J. Mol. Biol. 286*, 175−87.
55. Bracey, M. H., Hanson, M. A., Masuda, K. R., Stevens, R. C., and Cravatt, B. F. (2002) Structural adaptations in a membrane enzyme that terminates endocannabinoid signaling, *Science 298*, 1793−6.
56. Binda, C., Newton-Vinson, P., Hubalek, F., Edmondson, D. E., and Mattevi, A. (2002) Structure of human monoamine oxidase B, a drug target for the treatment of neurological disorders, *Nat. Struct. Biol. 9*, 22−6.
57. Colett, M. S., Larson, R., Gold, C., Strick, D., Anderson, D. K., and Purchio, A. F. (1988) Molecular cloning and nucleotide sequence of the pestivirus bovine viral diarrhea virus, *Virology 165*, 191−9.
58. Choo, Q. L., Richman, K. H., Han, J. H., Berger, K., Lee, C., Dong, C., Gallegos, C., Coit, D., Medina-Selby, R., Barr, P. J., et al. (1991) Genetic organization and diversity of the hepatitis C virus, *Proc. Natl. Acad. Sci. U.S.A. 88*, 2451−5.
59. Schneider, R., Unger, G., Stark, R., Schneider-Scherzer, E., and Thiel, H. J. (1993) Identification of a structural glycoprotein of an RNA virus as a ribonuclease, *Science 261*, 1169−71.
60. Wiskerchen, M., Belzer, S. K., and Collett, M. S. (1991) Pestivirus gene expression: The first protein product of the bovine viral diarrhea virus large open reading frame, p20, possesses proteolytic activity, *J. Virol. 65*, 4508−14.

BI0517685